

Precise dating of deglacial Laptev Sea sediments via ^{14}C and authigenic $^{10}\text{Be}/^9\text{Be}$ – assessing local ^{14}C reservoir ages

Arnaud Nicolas^{1,2}, Gesine Mollenhauer^{1,2,3}, Johannes Lachner⁴, Konstanze Stübner⁴, Maylin Malter¹, Jutta Wollenburg¹, Hendrik Grotheer^{1,3}, Florian Adolphi^{1,2}

¹Alfred Wegener Institute, Bremerhaven, Germany

²Department of Geosciences, University of Bremen, Bremen, Germany

³MARUM-Center for Marine Environmental Sciences, University of Bremen, Bremen, Germany

⁴Helmholtz-Zentrum Dresden-Rossendorf, Dresden, Germany

Correspondence: Arnaud Nicolas (arnaud.nicolas@awi.de) and Florian Adolphi (florian.adolphi@awi.de)

Abstract

Establishing accurate chronological frameworks is imperative for reliably identifying lead-lag dynamics within the climate system and enabling meaningful inter-comparisons across diverse paleoclimate proxy records over long time periods. Robust age models provide a solid temporal foundation for establishing correlations between paleoclimate records. One of the primary challenges in constructing reliable radiocarbon-based chronologies in the marine environment is to determine the regional marine radiocarbon reservoir age correction. Calculations of the local marine reservoir effect (ΔR) can be acquired using ^{14}C -independent dating methods, such as synchronization with other well-dated archives. The cosmogenic radionuclide ^{10}Be offers such a synchronization tool. Its atmospheric production rate is controlled by the global changes in the cosmic ray influx, caused by variations in solar activity and geomagnetic field strength. The resulting fluctuations in the meteoric deposition of ^{10}Be are preserved in sediments and ice cores and can thus be utilized for their synchronization. In this study, for the first time, we use the authigenic $^{10}\text{Be}/^9\text{Be}$ record of a Laptev Sea sediment core for the period 8-14 kyr BP and synchronize it with the ^{10}Be records from absolutely dated ice cores. Based on the resulting absolute chronology, a benthic ΔR value of $+345 \pm 60$ ^{14}C years was estimated for the Laptev Sea, which corresponds to a marine reservoir age of 848 ± 90 ^{14}C years. The ΔR value was used to refine the age-depth model for core PS2458-4, establishing it as a potential reference chronology for the Laptev Sea. We also compare the calculated ΔR value with modern estimates from the literature and discuss its implications for the age-depth model.

1 Introduction

Paleoclimate reconstructions can provide useful information about the dynamics of the climate system under different boundary conditions. Investigating how the climate variations propagate in space and time can provide important information about the underlying driving mechanisms (Adolphi et al., 2018; Czymzik et al., 2016b, a; Reinig et al., 2021). To correctly assess regional variations and spatio-temporal patterns in climate fluctuations, it is crucial to construct precise chronological frameworks. These frameworks serve as the temporal backbone for establishing correlations between paleoclimate records derived from marine, terrestrial, and ice-core archives. However, uncertainties in chronologies across different paleoclimate records often hinder the precise assessment of paleoclimate dynamics involving multiple records from different sites and archives (Southon, 2002).

One of the key challenges for constructing precise chronologies in the marine realm is to estimate the regional marine radiocarbon reservoir age correction, especially in polar regions (Alves et al., 2018; Heaton et al., 2023).

46 For constructing an age-depth model using ^{14}C dates of marine samples, it is crucial to include a precise marine
47 reservoir age (MRA). The MRA is the radiocarbon age difference between a marine sample and its contemporary
48 atmosphere (Stuiver et al., 1986). According to the most recent radiocarbon calibration curve, Marine20, the global
49 average marine reservoir age is approximately 500 ^{14}C years during the Holocene period (0 - 11.6 kyr BP) (Heaton
50 et al., 2020). However, regional differences in ocean-atmosphere exchange and internal ocean mixing can result
51 in large regional deviations from this global mean (Heaton et al., 2023). Therefore, the local marine reservoir
52 effect, ΔR was introduced and is defined as the difference between the regional and the modelled global marine
53 reservoir ages (Reimer and Reimer, 2001; Stuiver et al., 1986).

54

55 There is only one study that has provided modern MRA estimates for the Laptev Sea (Bauch et al., 2001). In this
56 study, the MRAs range from 295 ± 45 to 860 ± 55 ^{14}C years, with a mean value of 451 ± 72 ^{14}C years. Estimates
57 for MRA from the early deglaciation (~15 kyr BP) to the Holocene period for creating reliable deglacial
58 chronologies in the Laptev Sea are so far not available.

59

60 In order to provide estimates of the local ΔR back in time the samples must be independently dated by other means
61 than ^{14}C . This can for example be achieved by synchronization to other well-dated archives. Cosmogenic
62 radionuclides such as ^{10}Be and provide such a synchronization tool (Adolphi et al., 2018; Adolphi and Muscheler,
63 2016; Czymzik et al., 2018, 2020; Muscheler et al., 2014; Southon, 2002).

64

65 The cosmogenic radionuclides Beryllium-10 (^{10}Be , half-life = 1.387 ± 0.012 Myr) (Chmeleff et al., 2010;
66 Korschinek et al., 2010) and Carbon-14 (^{14}C , half-life = 5.700 ± 0.03 kyr) (Audi et al., 2003) are mainly produced
67 in Earth's upper atmosphere in a particle cascade that is triggered when galactic cosmic rays interact with atoms
68 in the atmosphere (Lal and Peters, 1967; Dunai and Lifton, 2014). The flux of these cosmic rays reaching Earth
69 is controlled by variations in the heliomagnetic and geomagnetic shielding (Lal and Peters, 1967; Masarik and
70 Beer, 1999) During periods of higher solar activity and/or geomagnetic field strength, production rates of ^{10}Be
71 and ^{14}C are decreased, whereas the production rates are higher during reduced solar activity and/or lower magnetic
72 field strength. The production rates of both cosmogenic radionuclide isotopes co-vary globally due to these
73 external processes.

74

75 Following production in the atmosphere, ^{14}C oxidizes to $^{14}\text{CO}_2$, enters the global carbon cycle and is incorporated
76 in environmental archives such as tree-rings, foraminifera, or speleothems. Annually, gigatons of carbon are
77 exchanged between the Earth's active reservoirs of the atmosphere, biosphere and the ocean, within the global
78 carbon cycle. Carbon is recycled and reused within these reservoirs and some reservoirs such as the deep ocean
79 can take hundreds of years to recycle carbon back to the atmosphere. The resulting heterogenous distribution of
80 radiocarbon among the different reservoirs stress the importance to understand and determine precise reservoir
81 ages.

82

83 In the atmosphere, the production of ^{10}Be in the more stably layered stratosphere is higher than in the troposphere.
84 About 63 % of ^{10}Be is produced in the stratosphere, 30 % in the tropical and subtropical troposphere together and
85 7 % in the polar troposphere (Adolphi et al., 2023; Poluianov et al., 2016). ^{10}Be is adsorbed onto aerosol particles,

86 mixed during about 1-yr residence time in the stratosphere, and is then transported and deposited on Earth's
87 surfaces through wet and dry deposition (Raisbeck et al., 1981; Zheng et al., 2023). The ^{10}Be production rates are
88 highest in the high-latitude stratosphere due to the weaker shielding of the cosmic ray flux by the Earth's magnetic
89 field. However, the highest ^{10}Be fluxes to Earth's surface are recorded in mid-latitudes because of the strong
90 regional exchange between stratosphere and troposphere and high precipitation rates leading to strong aerosol
91 scavenging (Heikkilä et al., 2013). Non-production processes such as variations in mixing, transport and
92 deposition of ^{10}Be and ^{14}C can complicate the reconstruction of cosmogenic radionuclide production rates from
93 paleoenvironmental archives. However, common variations in both cosmogenic radionuclide records are
94 considered to represent the cosmogenic radionuclide production signal, due to their common production
95 mechanism and different chemical behavior (Lal and Peters, 1967; Muscheler et al., 2008). ^{10}Be production rate
96 changes are relatively well-known from independently dated ice-core records (Finkel and Nishiizumi, 1997; Yiou
97 et al., 1997), and this can serve as a synchronization target for other records of ^{10}Be production rate changes.

98

99 In order to obtain reliable records of ^{10}Be -production rate changes from marine sediments, the effects of variable
100 sedimentation rates and particle scavenging must be accounted for, which can be efficiently achieved by
101 measuring authigenic $^{10}\text{Be}/^9\text{Be}$ (Bourles et al. 1989). The stable isotope ^9Be is a trace component in all continental
102 rocks. It is released by weathering of silicate rocks and transported to the ocean mainly by rivers (von
103 Blanckenburg et al., 2015). ^9Be (and to a lesser extent meteoric ^{10}Be) is introduced into the ocean in its dissolved
104 form where it is mixed with dissolved ^{10}Be of ocean water (mainly derived from atmospheric fallout, see above).
105 Since Be is particle reactive in seawater, dissolved $^{10}\text{Be}/^9\text{Be}$ is incorporated in marine authigenic phases as
106 amorphous coating on sediment or it can be preserved in authigenic Fe-Mn oxyhydroxides (von Blanckenburg
107 and Bouchez, 2014). Therefore, in marine sediment the authigenic $^{10}\text{Be}/^9\text{Be}$ ratio reflects the isotope ratio of
108 dissolved Be of the overlying water column at the time of sediment deposition (Bourles et al., 1989; von
109 Blanckenburg and Bouchez, 2014).

110

111 If the riverine input of ^9Be remains relatively constant, ^9Be and ^{10}Be are well-mixed (i.e., at sites >200 km from
112 the coast) (Wittmann et al., 2017), and the mixing of prevalent water-masses does not change, then authigenic
113 $^{10}\text{Be}/^9\text{Be}$ should primarily reflect changes in the cosmogenic production rates of ^{10}Be . In the Arctic Ocean, the
114 spatial patterns of $^{10}\text{Be}/^9\text{Be}$ in the water column are more heterogeneous than most other open ocean settings
115 because of the mixing of Atlantic waters with $^{10}\text{Be}/^9\text{Be}$ values of $5 - 10 \times 10^{-8}$ and Arctic Rivers with $^{10}\text{Be}/^9\text{Be}$
116 values of $0.3 - 1.5 \times 10^{-8}$ (Frank et al., 2009).

117

118 The aim of this study is to explore the use of an authigenic $^{10}\text{Be}/^9\text{Be}$ of a Laptev Sea sediment core for its
119 synchronization to ^{10}Be -records from absolutely dated ice cores. Using this result, we aim to infer the the local
120 marine reservoir effect, ΔR for the Laptev Sea during the deglaciation. This is the first study to exploit variations
121 in ^{10}Be production rates from Arctic marine sediments for stratigraphic purposes.

122

123

124

125

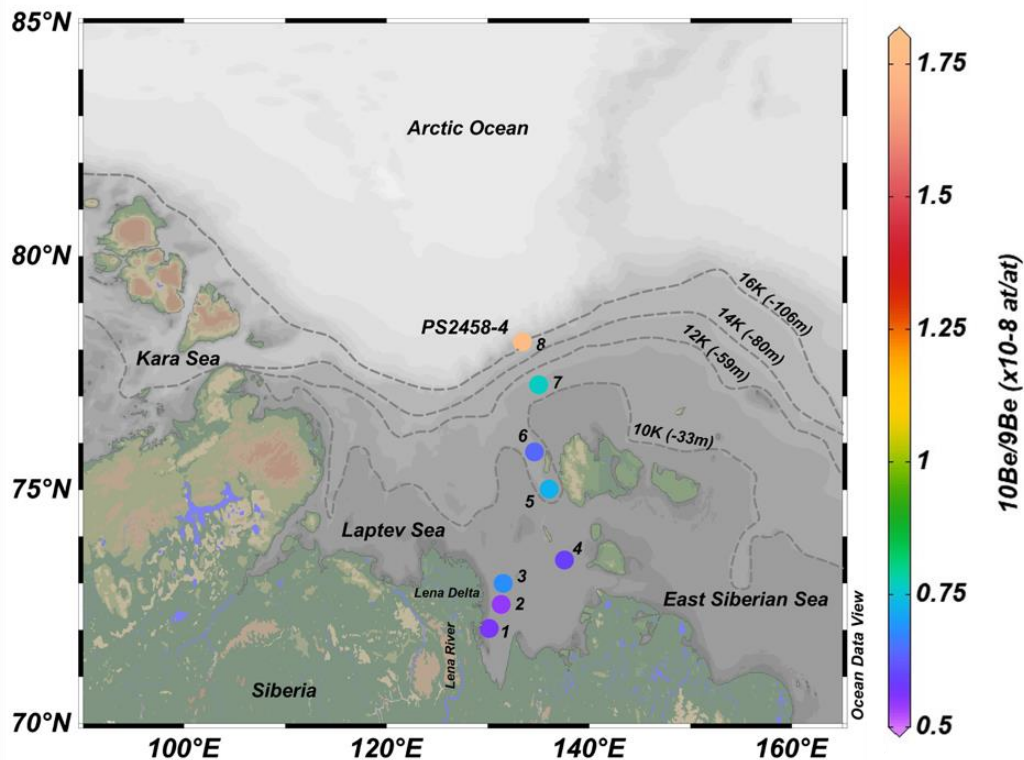
126

127

128 **2 Materials and methods**

129 **2.1 Sediment core location and initial chronology**

130 The sediment core PS2458-4 measured for ^9Be and ^{10}Be in this study, was retrieved in 1994 from the eastern
131 Laptev Sea continental margin (78°10.0'N, 133°23.9'E) at a water depth of 983 m (Fütterer, 1994) and
132 approximately about 518 km from the Lena Delta (Fig. 1). The 8 m long core consists of very dark olive-grey silty
133 clay of dominantly terrigenous origin (Fütterer, 1994). This core consists of a continuous high-sedimentation-rate
134 (77 cm /kyr) sequence representing the deglaciation period between approximately 16.5 and 9.3 kyr BP, followed
135 by a lower-sedimentation-rate (27 cm /kyr) early Holocene sequence (Fahl and Stein, 2012). A first chronology
136 of core PS2458-4 was established by accelerator mass spectrometry (AMS) ^{14}C dating of calcareous foraminifera,
137 bivalves and wood samples for the sediment interval between 201 and 667 cm, corresponding to a time interval
138 between approximately 8.8 and 14.3 kilo-calendar years BP (kyr BP) (Spielhagen et al., 2005). To improve the
139 existing age-depth model, 7 new AMS ^{14}C dates from mixed benthic foraminifera were used in combination with
140 7 ^{14}C dates from mixed benthic foraminifera and bivalves from Spielhagen et al. (2005) and an initial age-model
141 was derived using OxCal4.4 (Ramsey, 2009) (see Table 2). The mixed bivalve species used in Spielhagen et al.
142 (2005) were described as *Thyasira* sp. and *Yoldiella* sp (Table S1). Both bivalve species typically occur in cold
143 water environments at continental margins and in areas of limited food supply, as is the Laptev Sea continental
144 margin. Concerning the mixed benthic foraminifera species, usually epibenthic species such as *Lobatula lobatula*
145 are preferred. Since this latter species is rare in our sediment samples, other species such as: *Cassidulina*
146 *neoteretis*, *Islandiella helenae* and *Islandiella norcrossi* were selected for radiocarbon dating. In the Arctic Ocean
147 all these species live close to the sediment surface (Wollenburg and Kuhnt, 2000; Wollenburg and Mackensen,
148 1998) and reflect the carbon and oxygen isotope record of the bottom water in their shells. The marine ^{14}C dates
149 were calibrated with the Marine20 curve (Heaton et al., 2020). An average local marine reservoir effect (ΔR) value
150 of -110 ± 28 ^{14}C years was used based on the nearest modern values from Bauch et al. (2001) available from the
151 online database: <http://calib.org/marine/>. This chronology provides the initial basis for the stratigraphic fine-tuning
152 using $^{10}\text{Be}/^9\text{Be}$ as described below.



154 **Figure 1: Map of the Laptev Sea shelf showing the location of core PS2458-4 with core-top $^{10}\text{Be}/^9\text{Be}$ concentration**
 155 **(numbered colored circle 8) and $^{10}\text{Be}/^9\text{Be}$ concentrations of modern surface sediments (numbered colored circles 1-7).**
 156 **The dashed lines represent the reconstructed coastline extent at 4 different time periods (where 16K=16 kyr BP) with**
 157 **corresponding water depth values in meters shown in brackets (Klemann et al., 2015) . The Map was created using**
 158 **Ocean Data View (Schlitzer, 2016)**

159 2.2 Modern surface sediment samples from Laptev Sea

160 Seven modern surface sediment samples collected in the Laptev Sea were also included in the analysis (Figure 1,
 161 Table 1). Surface sediments with sample IDs 1 to 6 were collected during the Transdrift expeditions I and II in
 162 1993 and 1994 using Van Veen grabs and large spade box corer (Kassens and Dmitrenko, 1995; Kassens and
 163 Karpuy, 1994). Sediment sample from core PS2728-2 with ID number 7 was recovered in 1995 with a large
 164 rectangular box sampler during the Arctic Expedition ARK-XI/1 (Rachor, 1997). The sediment samples used in
 165 this study are distributed along a transect from near to the Lena Delta towards the open ocean near the shelf break,
 166 close to where core PS2458-4 was retrieved.

167 2.3 Sample preparation and measurements

168 Fifty-four sediment samples were selected along core PS2458-4 and processed for Be isotope analysis at the
 169 Alfred Wegener Institute in Bremerhaven (Germany). According to the initial radiocarbon-based age model, the
 170 selected samples covered three large cosmogenic radionuclide production rate swings, as evidenced by ice core
 171 ^{10}Be and tree-ring ^{14}C records (e.g., Adolphi and Muscheler, 2016), that occurred between 8.5 and 11.5 kyr BP.
 172 The leaching of the authigenic Fe-Mn oxyhydroxides phase followed Gutjahr et al. (2007) with minor
 173 modifications. Sediment samples were freeze-dried, homogenised and ~1 g of sediment was treated with 1 M
 174 NaOAc and adjusted with HOAc to pH 4 to dissolve carbonates which were discarded. Subsequently, the
 175 sediments were leached using 0.04 M hydroxylamine ($\text{NH}_2\text{OH}\cdot\text{HCl}$) in 15% HOAc at 95 °C for 4 h. We did not

176 leach the exchangeable fraction as proposed by Gutjahr et al. (2007) as this contained less than 1 % of the Be
177 leached in the hydroxylamine fraction with a very similar $^{10}\text{Be}/^9\text{Be}$ ratio. An aliquot from the resulting leaching
178 solution was sampled for stable ^9Be measurements using an Atomic Emission Spectrophotometer at the Alfred
179 Wegener Institute in Bremerhaven, Germany (Thermo Fisher Scientific Inc., ICP-OES-iCAP7400), with an
180 internal Yttrium standard and standard addition. The remaining ^{10}Be aliquot solution was spiked with a precisely
181 weighed amount of ^9Be -carrier (200, 300 or 500 μL of 1000 mg/L carrier solution, LGC 998969-73, $^{10}\text{Be}/^9\text{Be} =$
182 $(3.74 \pm 0.31) \times 10^{-15}$ at/at) (Merchel et al., 2021). The purification of the samples largely followed the method
183 outlined by Simon et al. (2016). The samples were evaporated, dissolved in distilled HCl and NH_3 was added for
184 Be oxy-hydroxide precipitation from the solution at pH 8 - 9. The precipitate was recovered by centrifugation and
185 then dissolved in 1 mL distilled 10.2 M HCl before loading onto a column filled with 15 mL Dowex[®] 1 x 8 (100-
186 200 mesh) anion-exchange resin in order to remove Fe from the sample. Prior, the resin was rinsed with 20 mL
187 MilliQ[®] water and conditioned with 30 mL 10.2 M HCl. The sample was then loaded onto the column and eluted
188 using 30 mL 10.2 M HCl. A column filled with 10 mL 50 x 8 (100 - 200 mesh) cation-exchange resin was used to
189 separate Be from B and Al. The resin was treated with 20 mL MilliQ[®] water followed by 20 mL 1 M HCl. The
190 sample was loaded onto the column and the first 25 mL 1 M HCl eluent, which contain mainly B, were discarded.
191 Be was eluted and collected with the next addition of 90 mL 1 M HCl. The resulting Be oxy-hydroxides were
192 precipitated at pH 8 - 9 by addition of NH_3 , then separated by centrifugation and washed 3 times by rinsing with
193 MilliQ[®] water to remove all chlorides. The purified Be oxy-hydroxides were transferred into quartz vials, dried
194 at 80 °C overnight and finally calcinated to BeO at 900 °C for 2 h. The BeO was mixed with Nb powder (Nb:BeO
195 = 4 : 1 by weight) and pressed into a Cu cathode-holder for accelerator mass spectrometer (AMS) measurements.
196 One blank and one replicate were measured with each batch of samples in order to assess reproducibility and
197 background during the extraction procedure.

198 AMS measurements were performed at DREAMS (DREsden AMS) facility (Lachner et al., 2023; Rugel et al.,
199 2016). All measurements were done relative to the standard “SMD-Be-12” with a weighted mean value of $(1.704$
200 $\pm 0.030) \times 10^{-12}$ (Akhmadaliev et al., 2013). Authigenic $^{10}\text{Be}/^9\text{Be}$ was calculated from the AMS results, the known
201 amount of carrier, and the measured authigenic ^9Be -concentration from Inductively Coupled Plasma Atomic
202 Emission Spectroscopy (ICP-AES) (see Simon et al., 2016). Considering the recent age of the samples, we did
203 not correct for decay of ^{10}Be . The correction would be in the order of 0.5 % and is an order of magnitude lower
204 than our combined measurement precision.

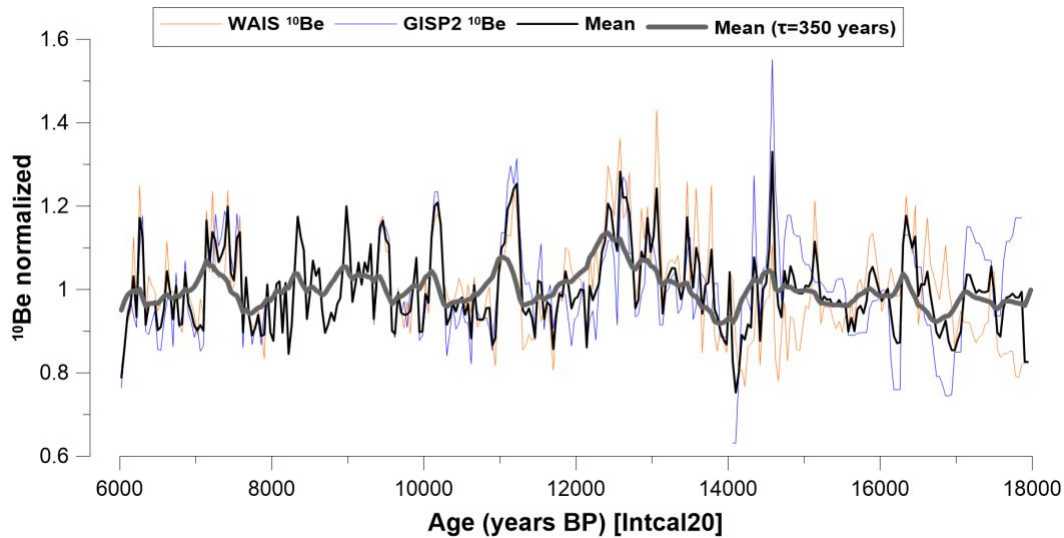
205 The preparation and measurement of the 7 new benthic foraminifera samples were undertaken based on the
206 standard operation procedures routinely used at the MICADAS ^{14}C laboratory facility of the Alfred Wegener
207 Institute (Mollenhauer et al., 2021). Prior to measurement, care was taken to critically select appropriate and
208 sufficient number of foraminifera shells without brownish discolouration or authigenic calcite overgrowth to
209 reduce uncertainty in the radiocarbon dates (Wollenburg et al., 2023).

210 **2.4 Ice core ^{10}Be record**

211 The ice core ^{10}Be record used in this study (Fig. 2) consists of normalized, averaged values of two ice cores: the
212 West Antarctic Ice Sheet (WAIS) Divide ice core ^{10}Be (Muschitiello et al., 2019; Sigl et al., 2016; Sinnl et al.,
213 2023) and the Greenland Ice Sheet Project Two (GISP2) ^{10}Be fluxes (Finkel and Nishiizumi, 1997). The ice core
214 fluxes had been corrected for climate influences by performing a regression against $\delta^{18}\text{O}$ and snow accumulation

215 rates (Adolphi et al., 2018). Prior to averaging, each ice core had been transferred to the IntCal20 timescale using
 216 the timescale transfer functions described in several previous studies (Adolphi and Muscheler, 2016; Adolphi et
 217 al., 2018 and Sigl et al., 2016). The glacial section of WAIS had been synchronized to Greenland Ice-Core
 218 Chronology 2005 (GICC05) by using volcanic (Svensson et al., 2020) and cosmogenic (Sinnl et al., 2023) tie
 219 points. The data from each ice core were resampled (averaged) to 40-year resolution before stacking. In order to
 220 facilitate a comparison between ice core and marine ^{10}Be changes, we modelled the expected marine signal from
 221 the ice core record following Christl (2007). We chose a 350-year residence time of Beryllium in the water column
 222 prior to deposition as this leads to a good agreement of amplitudes of the modelled centennial changes in ^{10}Be to
 223 the measured $^{10}\text{Be}/^9\text{Be}$ changes seen in the sediment. This 350-year residence time is within the range of values
 224 (80 ± 5 to 500 ± 25 years) reported in Arctic Ocean calculated from sedimentary fluxes and inventories (Frank et
 225 al., 2009).

226
227



228

229 **Figure 2: WAIS (orange)** (Muschitiello et al., 2019; Sigl et al., 2016; Sinnl et al., 2023) **and GISP2 (blue)** (Finkel and
 230 Nishiizumi, 1997) ^{10}Be fluxes corrected for correlation to ice core accumulation rates and $\delta^{18}\text{O}$, plotted on the IntCal20
 231 timescale. The thick black line shows the mean of both datasets and the bold grey line depicts the modelled oceanic ^{10}Be
 232 signal assuming a residence time (τ) of 350 years for ^{10}Be in the water column.

233

234 3 Results

235 The concentrations of ^9Be , ^{10}Be and $^{10}\text{Be}/^9\text{Be}$ atomic ratios from core PS2458-4 are displayed in Fig. 3 and the
 236 data are shown in Table S2. Five replicate samples of $^{10}\text{Be}/^9\text{Be}$ ratios are shown in Table S3. The agreement
 237 between these replicate measurements was assessed using the Coefficient of Variation (CV) for each depth. We
 238 observe that the authigenic $^{10}\text{Be}/^9\text{Be}$ ratios demonstrated relatively low CV values, ranging from 0.98% to 7.11%,
 239 which is in agreement with the stated uncertainties of the $^{10}\text{Be}/^9\text{Be}$ -ratio (Table S3). The dominant feature is an
 240 increasing trend of $^{10}\text{Be}/^9\text{Be}$ from the bottom to the top of the core. The modern surface sediment $^{10}\text{Be}/^9\text{Be}$ values
 241 ($[0.54 - 0.76] \times 10^{-8}$) from the offshore transect spanning from the Lena Delta to the core site (Table 1, Fig. 1) are
 242 consistent with $^{10}\text{Be}/^9\text{Be}$ of Lena water samples ($[0.62 \pm 0.07] \times 10^{-8}$) (Frank et al., 2009) and within the same
 243 range as PS2458-4 $^{10}\text{Be}/^9\text{Be}$ ($[0.53 - 1.77] \times 10^{-8}$). They show an increasing trend from the Lena Delta to the open

244 ocean (Fig. 1). The modern values close to the Lena are consistent with the lowest $^{10}\text{Be}/^9\text{Be}$ values of PS2458-4
 245 during the deglaciation, when the core-site was proximal to the paleo-river mouth of the Lena (see Figure 1).

246 **Table 1. Information about location, water depth, distance from Lena Delta and concentration of**
 247 **authigenic ^{10}Be , ^9Be , $^{10}\text{Be}/^9\text{Be}$ ratio leached of the modern surface sediment samples.**
 248

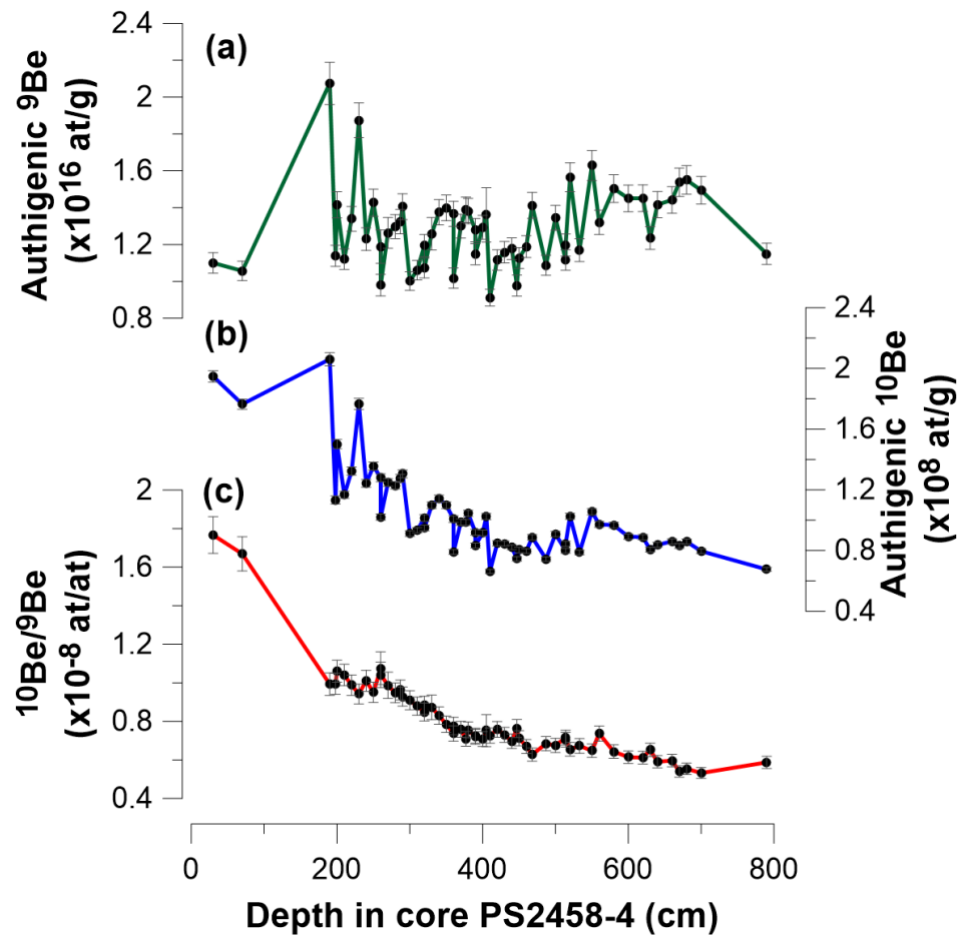
Sample name	Sample ID	Latitude (°)	Longitude (°)	Water Depth (m)	Approx. distance from Lena Delta (km)	^9Be (at/g) [$\times 10^{16}$]	^{10}Be (at/g) [$\times 10^8$]	$^{10}\text{Be}/^9\text{Be}$ (at/at) [$\times 10^{-8}$]
IK93Z4-4	1	72.03	130.13	14	28	1.12	0.63	0.56
IK9307-3	2	72.55	131.30	20.7	61	1.60	0.86	0.54
IK9316-6	3	73.00	131.50	27.8	65	1.89	1.15	0.61
IK9318-5	4	73.50	137.55	24	269	1.58	0.92	0.59
IK9350-6	5	75.02	136.03	31	295	1.13	0.82	0.72
IK9373A-6	6	75.81	134.58	46	322	1.46	0.93	0.64
PS2728-2a-1	7	77.25	135.01	44	471	1.42	1.09	0.76
PS2458-4*	8	78.17	133.38	983	518	1.28	1.95	1.77

*For core PS2458-4, the ^9B , ^{10}Be and $^{10}\text{Be}/^9\text{Be}$ results from the 30 cm sample are used as the core-top values.

249
 250 In order to use $^{10}\text{Be}/^9\text{Be}$ as a synchronization tool, we must remove this influence of mixing riverine and marine
 251 endmembers. It is non-trivial to derive a quantitative end-member mixing model solely from local sea-level
 252 reconstructions because sea-level only provides conceptual evidence about the variable proportions of open ocean
 253 and riverine water masses bathing the core site. Hence, we chose a statistical model, assuming that the changes in
 254 the endmember-mixing were gradual and hence, can be removed by normalizing to the long-term trend in the
 255 $^{10}\text{Be}/^9\text{Be}$ record. The residual centennial variability in $^{10}\text{Be}/^9\text{Be}$ is hypothesized to be driven by ^{10}Be -production
 256 rate changes and therefore suitable for synchronization.

257

258 Three different statistical models were used to test the sensitivity of our results to the choice of detrending
 259 techniques. Figure 4a illustrates the three different trend fitting techniques (logarithmic, power, and LOESS
 260 (LOcally Estimated Scatterplot Smoothing) applied to the $^{10}\text{Be}/^9\text{Be}$ data set. The relative $^{10}\text{Be}/^9\text{Be}$ residuals are
 261 plotted with respect to the logarithmic, power and LOESS trends (Fig. 4b) and the differences fall within the
 262 measurement uncertainties of the individual data points, showing that variations of the $^{10}\text{Be}/^9\text{Be}$ ratio are robust
 263 against the choice of the detrending model.



264

265 **Figure 3: Concentrations of (a) ^9Be , (b) ^{10}Be and (c) $^{10}\text{Be}/^9\text{Be}$ atomic ratios from core PS2458-4**

266

267

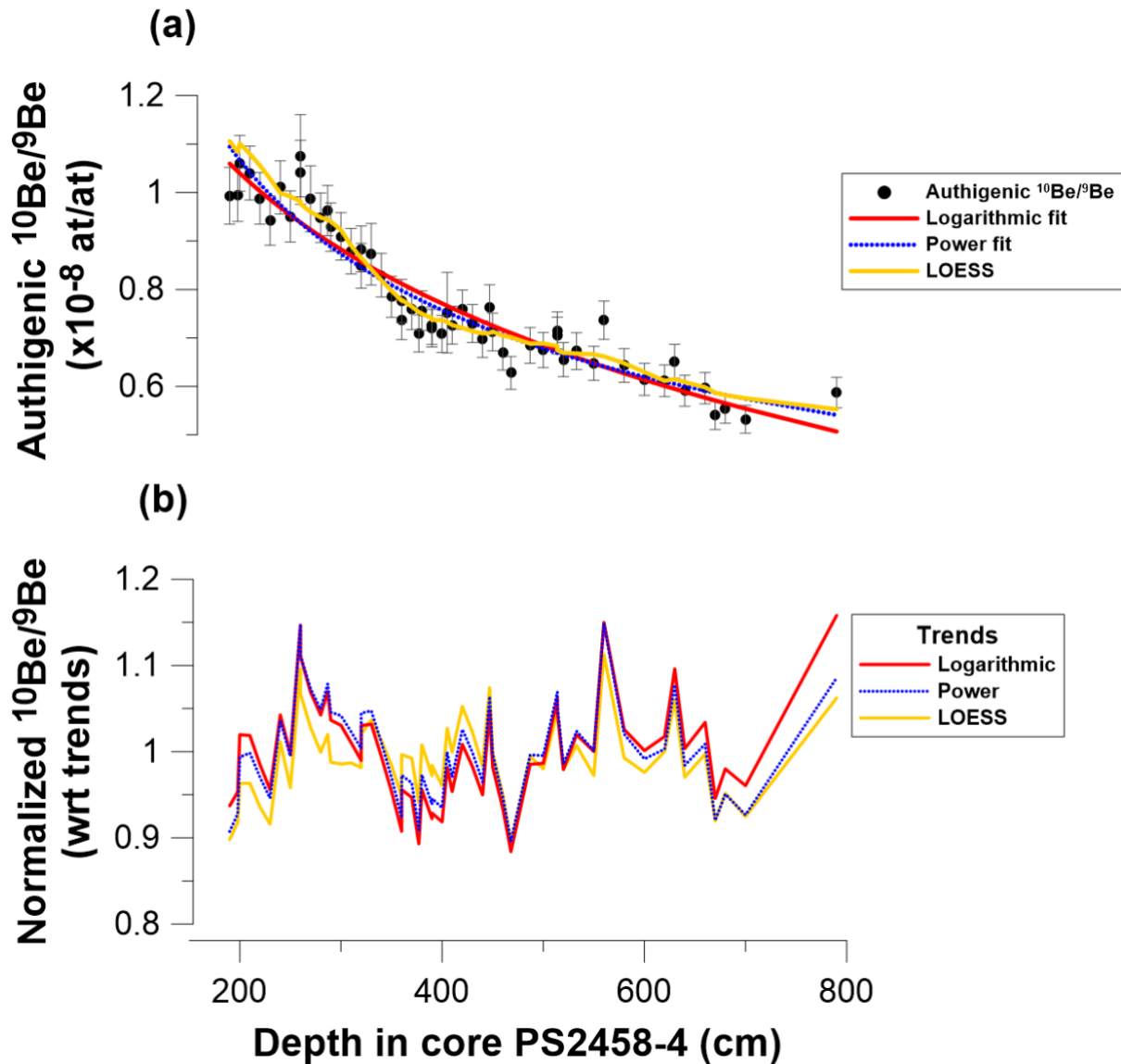


Figure 4: Sensitivity tests (a) Three different trend fitting techniques (logarithmic, power, and LOESS), (b) Relative $^{10}\text{Be}/^9\text{Be}$ residuals with respect to logarithmic, power and LOESS trends

268
269
270
271
272

To check whether the detrended $^{10}\text{Be}/^9\text{Be}$ record is driven by cosmogenic ^{10}Be production rate changes, we compare the detrended signal to the ice core ^{10}Be -record. Figure 5 shows the ice core ^{10}Be record and PS2458-4 mean profile of the three detrended data sets with a 3-point LOESS graph plotted on an initial ^{14}C -based age-scale (see used ΔR value below). Note however, that the following analyses have been performed on all three versions of the detrended dataset in order to test the robustness of our results against the choice of the detrending method. The variations observed in the sediment $^{10}\text{Be}/^9\text{Be}$ record follow closely the same pattern and relative amplitudes compared with the ice core ^{10}Be record. Therefore, we suggest that the variations observed in the $^{10}\text{Be}/^9\text{Be}$ record indeed reflect the production rate changes in the centennial range.

281

In order to refine the initial ^{14}C -based chronology and infer a regional deglacial ΔR -estimate, we constructed ^{14}C -based age-depth-models for PS2458-4 using OxCal 4.4 (Ramsey, 2009) assuming a range of ΔR between -110

283

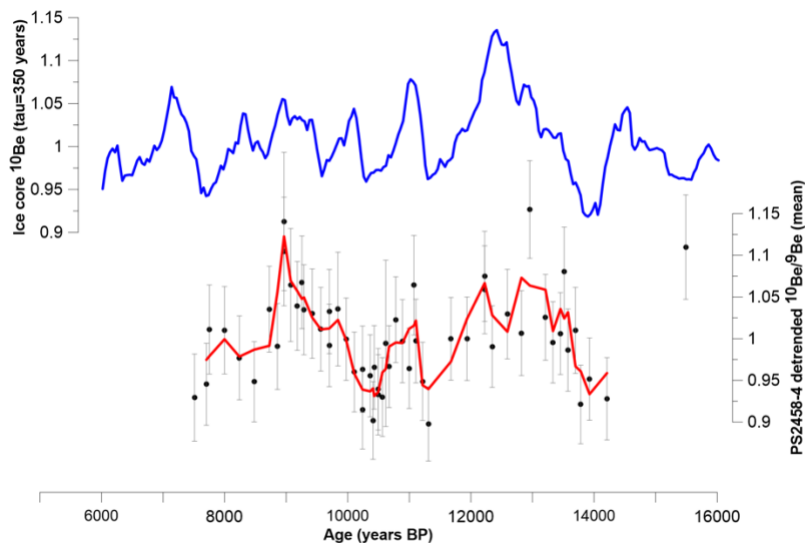
284 (Bauch et al., 2001) and +800 ¹⁴C years. Each age-model was then evaluated by comparing the resulting PS2458-
 285 4 ¹⁰Be/⁹Be-timeseries to the ice core ¹⁰Be-record. For this purpose, we use the generalized likelihood function by
 286 Christen and Pérez, (2009) that is otherwise used for the calibration of ¹⁴C-dates:
 287

$$288 \quad L_{\Delta R} \propto \prod_{j=1}^n \left[b + \frac{(x_j - y(t_j))^2}{2(\sigma_x^2 + \sigma_y^2)} \right]^{-(a+\frac{1}{2})}$$

289
 290 In our case, the ice core provides the calibration that describes ¹⁰Be-anomalies at each point in time (y(t)) which
 291 is compared to the sediment ¹⁰Be/⁹Be (x_j) on their modelled absolute age assuming a certain reservoir age. We use
 292 a = 3 and b = 4 based on the recommendation of Christen and Pérez (2009). This allows us to use ¹⁰Be to compare
 293 the likelihoods of different age models, and thus ¹⁴C-reservoir ages.
 294

295 The likelihood values were calculated for each of the three different trend fitting techniques and are shown in
 296 Figure 6. They result in a mean ΔR ± 1σ of 360 ± 75, 340 ± 50 and 335 ± 55 ¹⁴C years for the logarithmic, power
 297 and LOESS trend fitting techniques, respectively. These values are statistically indistinguishable and hence, we
 298 opt for the arithmetic mean ΔR value of 345 ± 60 ¹⁴C years. By using a global average marine reservoir age of
 299 503 ± 63 ¹⁴C years for the period 7.51-14.21 kyr BP (Heaton et al., 2020), we estimated a local MRA of 848 ± 90
 300 ¹⁴C years for the Laptev Sea during the deglaciation. The age-depth model for core PS2458-4 was reconstructed
 301 using radiocarbon dates of mixed benthic bivalves and benthic foraminifera (Spielhagen et al., 2005). Therefore,
 302 our calculated ΔR and corresponding MRA reflects to a benthic value.
 303

304 The depositional age-depth model with a ΔR value of 345 ± 60 ¹⁴C years for core PS2458-4 is shown in Figure
 305 S2 in the Supplement accompanying this manuscript. Compared to the mean modelled ages calculated with a ΔR
 306 value of -110 ± 28 ¹⁴C years, the new modelled ages computed with a ΔR value of 345 ± 60 ¹⁴C years were
 307 observed to shift younger in the range of 429 to 707 years (Table S1).



308
 309 **Figure 5: Ice core ¹⁰Be record with tau=350 years (blue) and PS2458-4 record calculated from the mean of the three**
 310 **detrended data sets with a 3-point LOESS graph using ΔR value of 345±60 ¹⁴C years for age-model (red)**

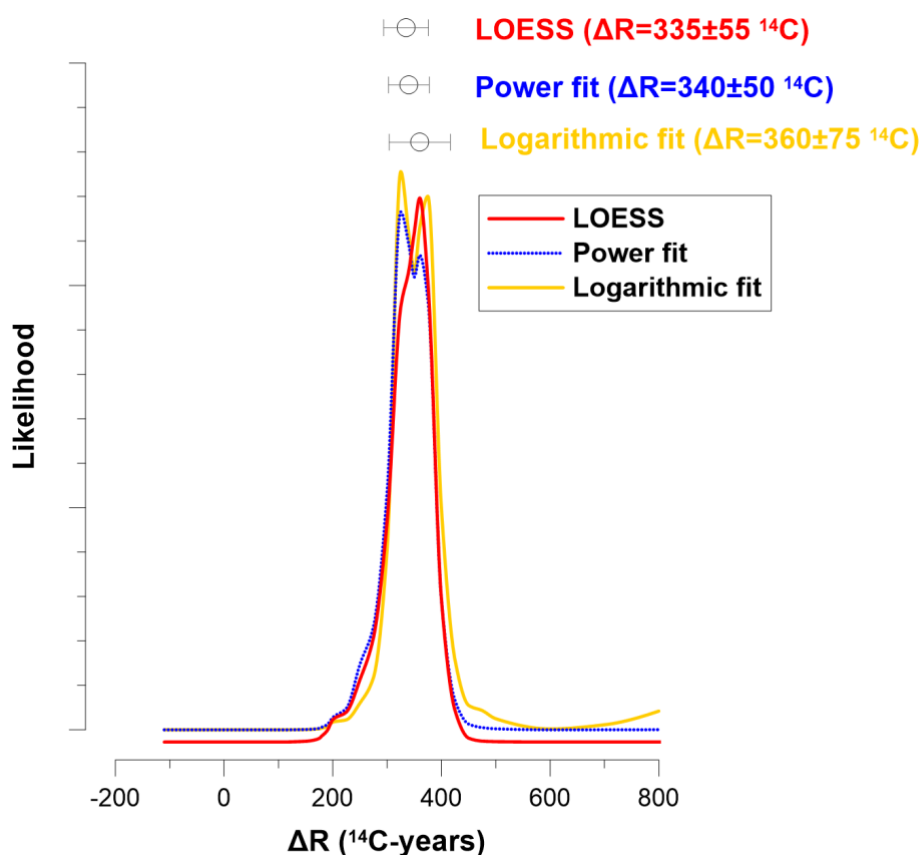
312
313
314
315

Figure 6: Likelihood results with mean $\Delta R \pm 1\sigma$ values of 360 ± 75 , 340 ± 50 and 335 ± 55 ^{14}C years BP based on LOESS (red), power (blue dotted) and logarithmic (yellow) trend fitting techniques respectively.

316

Table 2. Radiocarbon and modelled ages from foraminifera and bivalve samples from core PS2458-4

Depth (cm)	Sample ID	^{14}C Age (years)	\pm (years)	Modelled Age (mean) (cal BP)	Modelled Age (cal BP, 2σ)	Sample type
667	KIA6113	12600	110	13745	14089 – 13360	mb, mbf
578	AAR-3087	12270	65	13198	13428 – 12982	mb
530	AAR-3086	11560	100	12551	12815 – 12244	mb
491*	AWI-7415.1.1	10968	159	11753	12220 – 11280	mbf
467	AAR-3085	10600	75	11291	11630 – 11005	mb
399	AAR-3084	10090	65	10551	10811 – 10276	mb
369	AAR-3083	10020	70	10357	10606 – 10135	mb
331.5*	AWI-7412.1.1	9596	122	9860	10183 – 9527	mbf
291.5*	AWI-7411.1.1	9089	224	9305	9711 – 8917	mbf
252	AAR-3082	8830	55	8880	9129 – 8615	mb
241.5*	AWI-7410.1.1	8762	141	8762	9058 – 8448	mbf
141.5*	AWI-7409.1.1	6447	158	6334	6696 – 5969	mbf
121.5*	AWI-7408.1.1	6029	134	5985	6297 – 5638	mbf
0.5*	AWI-7786.3.1	0		0		mbf

Modelled ages were calculated using OxCal4.4 (Ramsey, 2009) with a ΔR value of 345 ± 60 ^{14}C years BP, as calculated in this study. Marine ^{14}C dates were calibrated with the Marine20 curve (Heaton et al., 2020). The depth values with asterisks represent the new benthic foraminifera samples measured for ^{14}C dates. The depth values without asterisks show the ^{14}C dates published from Spielhagen et al. (2005). Libby half-life (5568 years) was used to calculate ^{14}C age of foraminifera samples. Sample type: mb= mixed bivalves, mbf= mixed benthic foraminifera.

317

318

319 4 Discussion

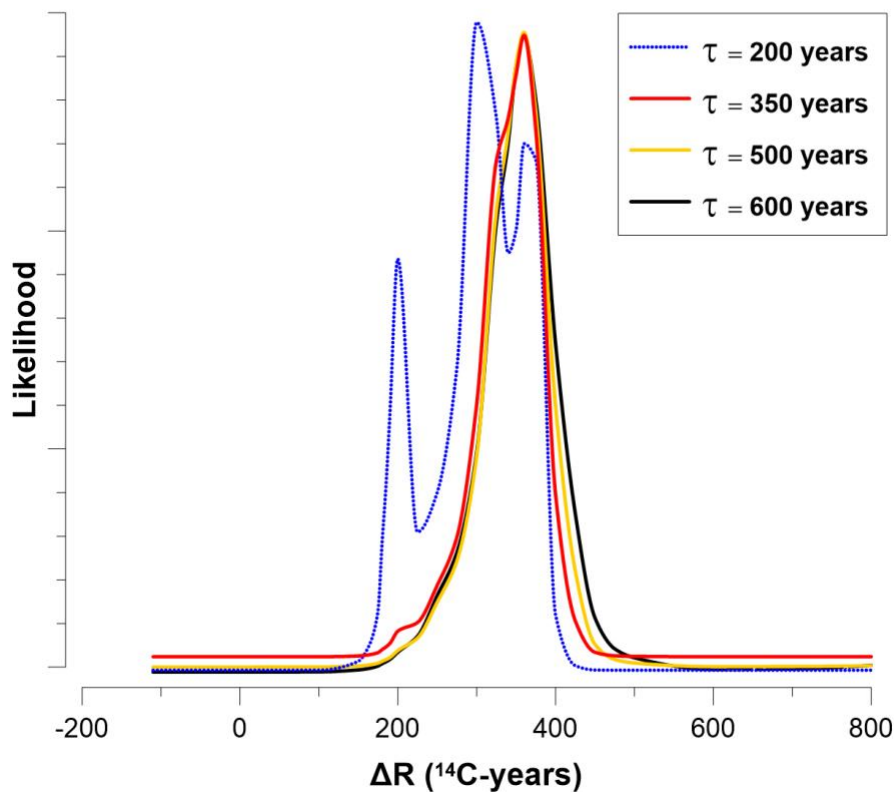
320 We have been able to quantitatively compare the agreement between ice core ^{10}Be and sediment $^{10}\text{Be}/^9\text{Be}$ for
321 different ΔR values and visually, we can observe how the two records representing cosmogenic radionuclide
322 production variations are in-phase with each other. It is a more robust approach to compare whole timeseries by
323 using a statistical method such as the likelihood function, instead of matching single wiggles or shorter time
324 periods with each other from both records. The latter method is more prone to noise in each dataset and
325 complicates the correct identification of matching peaks. By using just one single ΔR value of 345 ± 60 ^{14}C years,
326 we found that there is a strong agreement between both the ice core ^{10}Be and the sediment $^{10}\text{Be}/^9\text{Be}$ records. This
327 indirectly supports our constant ΔR assumption, which implies a constant offset from Marine20 rather than a
328 constant MRA (i.e., offset from IntCal20) throughout the studied period. Figure S2 illustrates the ^{14}C ages of
329 foraminifera samples plotted alongside with IntCal20 and Marine20 calibration curves. Figure S3 shows the non-
330 polar global-average MRA corresponding to Marine20 and the inferred MRA, calculated as the difference between
331 the atmospheric ^{14}C age (derived from IntCal20) and the ^{14}C age of foraminifera and bivalve samples. The inferred
332 MRA data points demonstrate close alignment with the Marine20 MRA+ ΔR data, indicating a robust correlation.
333 While this alignment is partially anticipated due to calibration with a constant ΔR , the agreement between the ^{14}C -
334 based age model and ^{10}Be data from ice core and sediment hence indicates that a time-variable ΔR is not required
335 to bring the ^{10}Be -records in agreement.

336
337 When modelling the ice core data, we have assumed a 350-year residence time of ^{10}Be in the water column prior
338 to deposition. We tested the influence of choosing different residence times of ^{10}Be in the water column when
339 modelling the ice core data and then synchronizing the modeled data sets with the PS2458-4 $^{10}\text{Be}/^9\text{Be}$ -timeseries.
340 Different tau values ($\tau = 200, 500, 600$ years) were used to model the ice core data and the ΔR -likelihood values
341 from the LOESS-smoothed ^{10}Be record were calculated. We observed that for all assumed tau-values likelihood
342 peaks occur at a ΔR value of 360 ^{14}C years (Fig. 7). This indicates that the most likely ΔR value is not strongly
343 dependent on the different assumed tau values. We found that only for the tau value of 200 years another best
344 likelihood estimate occurs at a ΔR value of 300 ^{14}C years BP, followed by the secondary likelihood maximum at
345 a ΔR value of 360 ^{14}C years BP. Figure S4 shows the modelled ice core time series with a tau value of 200 years,
346 which indicates clearly larger ^{10}Be amplitudes than what was calculated with a tau value of 350 years, which are
347 larger than the $^{10}\text{Be}/^9\text{Be}$ changes seen in PS2458-4. Based on these results, it seems unlikely that the best likelihood
348 estimate occurring at a ΔR value of 300 ^{14}C years BP with tau=200 years is real.

349
350 Our calculated local benthic MRA value of 848 ± 90 ^{14}C years BP is consistent with the modern values calculated
351 by Bauch et al. (2001), which range from 295 ± 45 to 860 ± 55 ^{14}C years. The largest modern reservoir age of 860
352 ± 55 ^{14}C years is located closest to the Lena Delta, which is comparable to the setting of the location of core
353 PS2458-4 during deglaciation around 14 - 12 kyr BP. Another study from the central Arctic Ocean reported MRA
354 values of 1400 ^{14}C years BP ($\Delta R = 1000$) during the Late Glacial and 700 ^{14}C years BP ($\Delta R = 300$) during the
355 Holocene (Hanslik et al., 2010).

356
357 The ΔR value was calculated during the deglaciation (14-8 kyr BP) and during this period the mean relative sea
358 level rose by about 64 m (Klemann et al., 2015). The core was retrieved at a depth of 983 m in 1994 and at 14 and

359 8 kyr BP the depths were about 903 and 967 m respectively. Moreover, as shown in Figure 1, the modern surface
 360 $^{10}\text{Be}/^9\text{Be}$ values show an increasing trend from the Lena Delta to the open ocean (Fig. 1). Thus, we attribute the
 361 trend in PS2458-4 $^{10}\text{Be}/^9\text{Be}$ to deglacial sea level rise and the associated coastline retreat (Bauch et al., 2001;
 362 Klemann et al., 2015). During the glacial period, the core site was located close to the Lena River mouth and
 363 hence, bathed in river-water with low $^{10}\text{Be}/^9\text{Be}$. With increasing sea-level and coastline retreat, open ocean waters
 364 with higher $^{10}\text{Be}/^9\text{Be}$ became more dominant.



365
 366 **Figure 7. Likelihood results based on different ΔR for the LOESS-smoothed ice core ^{10}Be using for different tau values**
 367 **of 200, 350, 500 and 600 years.**

368
 369 We compared our estimated ΔR value 345 ± 60 ^{14}C years with the approach proposed by Heaton et al. (2023) to
 370 infer glacial ΔR values in polar regions. In the polar regions (outside $40^\circ \text{S} - 40^\circ \text{N}$), it is expected that during
 371 glacial episodes, there may have been regional differences in the amount of oceanic ^{14}C depletion compared to
 372 the global non-polar ocean mean represented by Marine20. The increase in the volume and density of sea ice
 373 limiting air-sea gas-exchange may cause a significant larger ΔR during the glacial era compared to the interglacial
 374 values. For glacial periods (55.0 - 11.5 kyr BP), Heaton et al. (2023) proposed a latitude-dependent method to
 375 infer upper bounds of the possible ΔR difference between Holocene and Glacial in polar regions. A lower bound
 376 ΔR^{Hol} is based on samples from the Holocene and an upper (glacial) bound ΔR^{GS} , is calculated by increasing ΔR^{Hol}
 377 depending on the latitude.

378

379 The PS2458-4 record used in this study extends from about 7.5 to 14.2 kyr BP and therefore covers the early
380 Holocene and parts of the deglacial period. Thus, from 11.5 to 14.2 kyr BP, the record extends into the glacial and
381 samples from this period may require a glacial polar boost as proposed by Heaton et al. (2023). We calculated
382 ΔR^{Hol} from ^{14}C samples found in the online database at <http://calib.org/marine/> (Reimer and Reimer, 2001). Using
383 the weighed mean value of the 5 nearest ΔR values from the core location in the Laptev Sea from Bauch et al.
384 (2001), yields a ΔR^{Hol} value of -95 ± 61 ^{14}C years. ΔR^{GS} was calculated as: $\Delta R^{\text{GS}} = \Delta R^{\text{Hol}} + \Delta R^{\text{Hol} \rightarrow \text{GS}}$, in agreement
385 with the GS scenario as described in Heaton et al. (2023). The value $\Delta R^{\text{Hol} \rightarrow \text{GS}}$ is dependent on the latitude of the
386 sample and at 78.75°N , it amounts to 790 ^{14}C years. The resulting ΔR^{GS} value is 695 ± 61 ^{14}C years and is much
387 larger than our inferred benthic ΔR value (345 ± 60 ^{14}C years).

388
389 These differences are likely due to distinct regional changes in climate and hydrology. At the core location in the
390 Laptev Sea, sea-ice cover was less during the Younger Dryas and Heinrich Stadial 1 compared to the Holocene
391 (Fahl and Stein, 2012), contrary to large-scale deglacial sea ice trends included in the model by Heaton et al.
392 (2023). The expansion of regional sea-ice cover during the recent past in the Laptev Sea could have further
393 influenced the ΔR value, which then should have been larger during the Holocene compared to the early
394 deglaciation. However, our calculated ΔR value of 345 ± 60 ^{14}C years is larger than the modern average ΔR value
395 of -95 ± 61 ^{14}C years, making it unlikely that sea-ice cover dynamics were the main driver of past changes in
396 regional ΔR . Instead, as mentioned before, the local reservoir ages in the region are spatially highly variable and
397 influenced by a hardwater effect (Bauch et al. 2001). These regional processes are thus site specific and hence,
398 obviously cannot be covered by the approach of Heaton et al. (2023). Bauch et al. (2001) reported that the
399 relatively old ^{14}C -age of bivalve shells collected in proximity of the Lena Delta near Tiksi Bay, might be due to
400 the influence of local hardwater effect. This is consistent with the modern setting where the largest ΔR is found
401 close to the Lena Delta and lower ΔR towards the shelf-edge (Bauch et al., 2001). Hence, the larger deglacial ΔR
402 of PS2458-4 could be driven by its proximity to the Lena River during that time as evidenced by low $^{10}\text{Be}/^9\text{Be}$ as
403 discussed earlier.

404
405

406 **5 Conclusion**

407 We present high-resolution ^9Be and ^{10}Be records reconstructed from core PS2458-4, which was retrieved from the
408 continental slope of the eastern Laptev Sea in the Arctic Ocean. We demonstrate that these records are influenced
409 by the distance of the core site to the Lena River, which changed depending on sea-level. Centennial to millennial
410 scale variability in the $^{10}\text{Be}/^9\text{Be}$ ratio can be attributed to variations in production rate and can hence be used to
411 correlate our sediment record to ice-core ^{10}Be records.

412
413 This is the first study to reconstruct high-resolution ^{10}Be production rate changes from $^{10}\text{Be}/^9\text{Be}$ records from
414 Arctic marine sediments for correlation to ice cores, and this approach has been applied with success. We have
415 correlated the ^{10}Be from marine sediment core PS2458-4 with ^{10}Be from ice core and used a likelihood function
416 to estimate ΔR values.

417

418 Our estimate for the deglacial benthic ΔR value for the Laptev Sea is 345 ± 60 ^{14}C years BP corresponding to a
419 MRA of 848 ± 90 ^{14}C years. The ΔR value will be used to refine the age-depth model for core PS2458-4 from the
420 Laptev Sea, which could be used as a reference chronology for the Laptev Sea.

421

422 **Data availability**

423

424 The ^9Be , ^{10}Be and $^{10}\text{Be}/^9\text{Be}$ data sets from core PS2458-4 generated in this study are available as a Supplement
425 to this paper.

426

427 **Author contributions**

428

429 FA and GM designed the study. AN, MM conducted the laboratory analyses and FA, AN and GM analyzed the
430 data. JL and KS were responsible for preparation and conduction of the ^{10}Be AMS measurements. JW selected
431 appropriate foraminifera samples for radiocarbon dating. HG undertook the radiocarbon measurement of the
432 foraminifera samples and analyzed the data. AN drafted a first version of the paper and FA and AN generated the
433 figures. All co-authors contributed to the writing and provided feedback on the paper.

434

435 **Competing interests**

436

437 The contact author has declared that neither of the authors has any competing interests.

438

439

440 **Acknowledgements**

441

442 Parts of this research were carried out at the Ion Beam Centre (IBC) at the Helmholtz-Zentrum Dresden-
443 Rossendorf e. V., a member of the Helmholtz Association. We would like to thank the DREAMS operator team
444 for their assistance with AMS-measurements. FA was supported by the Helmholtz Association (VH-NG 1501).
445 We are grateful for the technical support offered by Torben Gentz and Elizabeth Bonk from the MICADAS facility
446 at AWI Bremerhaven. AN would like to thank DAAD and POLMAR for support during his doctoral studies.

447

448

449

450

451

452

453

454

455

456

457

458

459

460

461

462

463

464

465

466 **References**

- 467 Adolphi, F. and Muscheler, R.: Synchronizing the Greenland ice core and radiocarbon timescales over the
468 Holocene-Bayesian wiggle-matching of cosmogenic radionuclide records, *Climate of the Past*, 12, 15–30,
469 <https://doi.org/10.5194/cp-12-15-2016>, 2016.
- 470 Adolphi, F., Bronk Ramsey, C., Erhardt, T., Edwards, R. L., Cheng, H., Turney, C. S. M., Cooper, A., Svensson, A.,
471 Rasmussen, S. O., Fischer, H., and Muscheler, R.: Connecting the Greenland ice-core and U/Th timescales via
472 cosmogenic radionuclides: testing the synchronicity of Dansgaard–Oeschger events, *Climate of the Past*, 14,
473 1755–1781, <https://doi.org/10.5194/cp-14-1755-2018>, 2018.
- 474 Adolphi, F., Herbst, K., Nilsson, A., and Panovska, S.: On the Polar Bias in Ice Core 10Be Data, *Journal of*
475 *Geophysical Research: Atmospheres*, 128, <https://doi.org/10.1029/2022JD038203>, 2023.
- 476 Akhmadaliev, S., Heller, R., Hanf, D., Rugel, G., and Merchel, S.: The new 6MV AMS-facility DREAMS at
477 Dresden, *Nucl Instrum Methods Phys Res B*, 294, 5–10, <https://doi.org/10.1016/j.nimb.2012.01.053>, 2013.
- 478 Alves, E. Q., Macario, K., Ascough, P., and Bronk Ramsey, C.: The Worldwide Marine Radiocarbon Reservoir
479 Effect: Definitions, Mechanisms, and Prospects, *Reviews of Geophysics*, 56, 278–305,
480 <https://doi.org/https://doi.org/10.1002/2017RG000588>, 2018.
- 481 Audi, G., Bersillon, O., Blachot, J., and Wapstra, A. H.: The NUBASE evaluation of nuclear and decay properties,
482 *Nucl Phys A*, 729, <https://doi.org/10.1016/j.nuclphysa.2003.11.001>, 2003.
- 483 Bauch, H. A., Mueller-Lupp, T., Taldenkova, E., Spielhagen, R. F., Kassens, H., Grootes, P. M., Thiede, J.,
484 Heinemeier, J., and Petryashov, V. V.: Chronology of the holocene transgression at the north siberian margin,
485 *Glob Planet Change*, 31, [https://doi.org/10.1016/S0921-8181\(01\)00116-3](https://doi.org/10.1016/S0921-8181(01)00116-3), 2001.
- 486 Von Blanckenburg, F. and Bouchez, J.: River fluxes to the sea from the ocean’s 10Be/9Be ratio, *Earth Planet Sci*
487 *Lett*, 387, 34–43, <https://doi.org/10.1016/j.epsl.2013.11.004>, 2014.
- 488 von Blanckenburg, F., Bouchez, J., Ibarra, D. E., and Maher, K.: Stable runoff and weathering fluxes into the
489 oceans over Quaternary climate cycles, *Nat Geosci*, 8, 538–542, <https://doi.org/10.1038/ngeo2452>, 2015.
- 490 Bourles, D., Raisbeck, G. M., and Yiou, F.: 10Be and 9Be in marine sediments and their potential for dating, 443–
491 452 pp., 1989.
- 492 Chmeleff, J., von Blanckenburg, F., Kossert, K., and Jakob, D.: Determination of the 10Be half-life by
493 multicollector ICP-MS and liquid scintillation counting, *Nucl Instrum Methods Phys Res B*, 268, 192–199,
494 <https://doi.org/10.1016/j.nimb.2009.09.012>, 2010.
- 495 Christen, A. J. and Pérez, S. E.: A new robust statistical model for radiocarbon data, *Radiocarbon*, 51,
496 <https://doi.org/10.1017/s003382220003410x>, 2009.
- 497 Christl, M.: Sensitivity and response of beryllium-10 in marine sediments to rapid production changes
498 (geomagnetic events): A box model study, *Geochemistry, Geophysics, Geosystems*, 8,
499 <https://doi.org/10.1029/2007GC001598>, 2007.
- 500 Czymzik, M., Dreibrodt, S., Feeser, I., Adolphi, F., and Brauer, A.: Mid-Holocene humid periods reconstructed
501 from calcite varves of the Lake Woserin sediment record (north-eastern Germany), *Holocene*, 26, 935–946,
502 <https://doi.org/10.1177/0959683615622549>, 2016a.
- 503 Czymzik, M., Muscheler, R., and Brauer, A.: Solar modulation of flood frequency in central Europe during spring
504 and summer on interannual to multi-centennial timescales, *Climate of the Past*, 12, 799–805,
505 <https://doi.org/10.5194/cp-12-799-2016>, 2016b.
- 506 Czymzik, M., Muscheler, R., Adolphi, F., Mekhaldi, F., Dräger, N., Ott, F., Slowinski, M., Blaszkiewicz, M.,
507 Aldahan, A., Possnert, G., and Brauer, A.: Synchronizing 10Be in two varved lake sediment records to IntCal13
508 14C during three grand solar minima, *Climate of the Past*, 14, 687–696, <https://doi.org/10.5194/cp-14-687-2018>,
509 2018.
- 510 Czymzik, M., Nowaczyk, N. R., Dellwig, O., Wegwerth, A., Muscheler, R., Christl, M., and Arz, H. W.: Lagged
511 atmospheric circulation response in the Black Sea region to Greenland Interstadial 10,
512 <https://doi.org/10.1073/pnas.2005520117/-/DCSupplemental>, 2020.
- 513 Dunai, T. J. and Lifton, N. A.: The nuts and bolts of cosmogenic nuclide production, *Elements*, 10, 347–350,
514 <https://doi.org/10.2113/gselements.10.5.347>, 2014.
- 515 Fahl, K. and Stein, R.: Modern seasonal variability and deglacial/Holocene change of central Arctic Ocean sea-ice
516 cover: New insights from biomarker proxy records, *Earth Planet Sci Lett*, 351–352, 123–133,
517 <https://doi.org/10.1016/j.epsl.2012.07.009>, 2012.
- 518 Finkel, R. C. and Nishiizumi, K.: Beryllium 10 concentrations in the Greenland Ice Sheet Project 2 ice core from
519 3-40 ka, *J Geophys Res Oceans*, 102, <https://doi.org/10.1029/97JC01282>, 1997.
- 520 Frank, M., Porcelli, D., Andersson, P., Baskaran, M., Björk, G., Kubik, P. W., Hattendorf, B., and Guenther, D.:
521 The dissolved Beryllium isotope composition of the Arctic Ocean, *Geochim Cosmochim Acta*, 73,
522 <https://doi.org/10.1016/j.gca.2009.07.010>, 2009.
- 523 Fütterer, D. K.: The expedition ARCTIC’93, Leg ARK-IX/4 of RV “Polarstern” 1993, Report on Polar Research,
524 149, 244pp., 1994.

525 Gutjahr, M., Frank, M., Stirling, C. H., Klemm, V., van de Flierdt, T., and Halliday, A. N.: Reliable extraction of a
526 deepwater trace metal isotope signal from Fe-Mn oxyhydroxide coatings of marine sediments, *Chem Geol*, 242,
527 351–370, <https://doi.org/10.1016/j.chemgeo.2007.03.021>, 2007.

528 Hanslik, D., Jakobsson, M., Backman, J., Björck, S., Sellén, E., O’Regan, M., Fornaciari, E., and Skog, G.:
529 Quaternary Arctic Ocean sea ice variations and radiocarbon reservoir age corrections, *Quat Sci Rev*, 29,
530 <https://doi.org/10.1016/j.quascirev.2010.06.011>, 2010.

531 Heaton, T. J., Köhler, P., Butzin, M., Bard, E., Reimer, R. W., Austin, W. E. N., Bronk Ramsey, C., Grootes, P. M.,
532 Hughen, K. A., Kromer, B., Reimer, P. J., Adkins, J., Burke, A., Cook, M. S., Olsen, J., and Skinner, L. C.:
533 Marine20 - The Marine Radiocarbon Age Calibration Curve (0-55,000 cal BP), *Radiocarbon*, 62,
534 <https://doi.org/10.1017/RDC.2020.68>, 2020.

535 Heaton, T. J., Butzin, M., Bard, E., Bronk Ramsey, C., Hughen, K. A., Kohler, P., and Reimer, P. J.: Marine
536 radiocarbon calibration in polar regions: A simple approximate approach using marine20, *Radiocarbon*, 65,
537 <https://doi.org/10.1017/RDC.2023.42>, 2023.

538 Heikkilä, U., Beer, J., Abreu, J. A., and Steinhilber, F.: On the atmospheric transport and deposition of the
539 cosmogenic radionuclides (^{10}Be): A review, <https://doi.org/10.1007/s11214-011-9838-0>, June 2013.

540 Kassens, H. and Dmitrenko, I.: Russian-German Cooperation: The TRANSDRIFT II expedition to the Laptev Sea.,
541 *Reports on Polar Research*, 182, 1–180, 1995.

542 Kassens, H. and Karpiy, V. Y.: Russian-German cooperation: the transdrift I expedition to the Laptev sea., *Reports*
543 *on Polar Research*, 151–168, 1994.

544 Klemann, V., Heim, B., Bauch, H. A., Wetterich, S., and Opel, T.: Sea-level evolution of the Laptev Sea and the
545 East Siberian Sea since the last glacial maximum, *arktos*, 1, <https://doi.org/10.1007/s41063-015-0004-x>, 2015.

546 Korschinek, G., Bergmaier, A., Faestermann, T., Gerstmann, U. C., Knie, K., Rugel, G., Wallner, A., Dillmann, I.,
547 Dollinger, G., von Gostomski, C. L., Kossert, K., Maiti, M., Poutivtsev, M., and Remmert, A.: A new value for
548 the half-life of ^{10}Be by Heavy-Ion Elastic Recoil Detection and liquid scintillation counting, *Nucl Instrum*
549 *Methods Phys Res B*, 268, 187–191, <https://doi.org/10.1016/j.nimb.2009.09.020>, 2010.

550 Lachner, J., Rugel, G., Vivo Vilches, C., Koll, D., Stübner, K., Winkler, S., and Wallner, A.: Optimization of ^{10}Be
551 measurements at the 6 MV AMS facility DREAMS, *Nucl Instrum Methods Phys Res B*, 535, 29–33,
552 <https://doi.org/10.1016/j.nimb.2022.11.008>, 2023.

553 Lal, D. and Peters, B.: Cosmic Ray Produced Radioactivity on the Earth. In: *Handbuch der Physik*, vol. XLVI/2.
554 Springer, New York, 551–612 pp., 1967.

555 Masarik, J. and Beer, J.: Simulation of particle fluxes and cosmogenic nuclide production in the Earth’s
556 atmosphere, *Journal of Geophysical Research Atmospheres*, 104, <https://doi.org/10.1029/1998JD200091>, 1999.

557 Merchel, S., Braucher, R., Lachner, J., and Rugel, G.: Which is the best ^9Be carrier for $^{10}\text{Be}/^9\text{Be}$ accelerator mass
558 spectrometry?, *MethodsX*, 8, <https://doi.org/10.1016/j.mex.2021.101486>, 2021.

559 Mollenhauer, G., Grotheer, H., Gentz, T., Bonk, E., and Hefter, J.: Standard operation procedures and performance
560 of the MICADAS radiocarbon laboratory at Alfred Wegener Institute (AWI), Germany, *Nucl Instrum Methods*
561 *Phys Res B*, 496, <https://doi.org/10.1016/j.nimb.2021.03.016>, 2021.

562 Muscheler, R., Kromer, B., Björck, S., Svensson, A., Friedrich, M., Kaiser, K. F., and Southon, J.: Tree rings and
563 ice cores reveal ^{14}C calibration uncertainties during the Younger Dryas, *Nat Geosci*, 1,
564 <https://doi.org/10.1038/ngeo128>, 2008.

565 Muscheler, R., Adolphi, F., and Knudsen, M. F.: Assessing the differences between the IntCal and Greenland ice-
566 core time scales for the last 14,000 years via the common cosmogenic radionuclide variations, *Quat Sci Rev*,
567 106, 81–87, <https://doi.org/10.1016/j.quascirev.2014.08.017>, 2014.

568 Muschitiello, F., D’Andrea, W. J., Schmittner, A., Heaton, T. J., Balascio, N. L., deRoberts, N., Caffee, M. W.,
569 Woodruff, T. E., Welten, K. C., Skinner, L. C., Simon, M. H., and Dokken, T. M.: Deep-water circulation
570 changes lead North Atlantic climate during deglaciation, *Nat Commun*, 10, <https://doi.org/10.1038/s41467-019-09237-3>, 2019.

572 Poluianov, S. V., Kovaltsov, G. A., Mishev, A. L., and Usoskin, I. G.: Production of cosmogenic isotopes ^7Be ,
573 ^{10}Be , ^{14}C , ^{22}Na , and ^{36}Cl in the atmosphere: Altitudinal profiles of yield functions, *J Geophys Res*, 121,
574 <https://doi.org/10.1002/2016JD025034>, 2016.

575 Rachor, E.: Scientific cruise report of the Arctic expedition ARK-XI/1 of RV “Polarstern” in 1995, *Reports on*
576 *Polar and Marine Research*, 226, 1–336, 1997.

577 Raisbeck, G. M., Yiou, F., Fruneau, M., Loiseaux, J. M., Lieuvin, M., and Ravel, J. C.: Cosmogenic $^{10}\text{Be}/^7\text{Be}$ as a
578 probe of atmospheric transport processes, *Geophys Res Lett*, 8, 1015–1018,
579 <https://doi.org/10.1029/GL008i009p01015>, 1981.

580 Ramsey, C. B.: Bayesian analysis of radiocarbon dates, *Radiocarbon*, 51,
581 <https://doi.org/10.1017/s0033822200033865>, 2009.

582 Reimer, P. J. and Reimer, R. W.: A marine reservoir correction database and on-line interface, *Radiocarbon*, 43,
583 <https://doi.org/10.1017/s0033822200038339>, 2001.

584 Reinig, F., Wacker, L., Jöris, O., Oppenheimer, C., Guidobaldi, G., Nievergelt, D., Adolphi, F., Cherubini, P.,
585 Engels, S., Esper, J., Land, A., Lane, C., Pfanz, H., Remmele, S., Sigl, M., Sookdeo, A., and Büntgen, U.:
586 Precise date for the Laacher See eruption synchronizes the Younger Dryas, *Nature*, 595,
587 <https://doi.org/10.1038/s41586-021-03608-x>, 2021.

588 Rugel, G., Pavetich, S., Akhmadaliev, S., Enamorado Baez, S. M., Scharf, A., Ziegenrucker, R., and Merchel, S.:
589 The first four years of the AMS-facility DREAMS: Status and developments for more accurate radionuclide
590 data, *Nucl Instrum Methods Phys Res B*, 370, 94–100, <https://doi.org/10.1016/j.nimb.2016.01.012>, 2016.

591 Schlitzer, R.: Ocean Data View, <https://odv.awi.de>, 2016.

592 Sigl, M., Fudge, T. J., Winstrup, M., Cole-Dai, J., Ferris, D., McConnell, J. R., Taylor, K. C., Welten, K. C.,
593 Woodruff, T. E., Adolphi, F., Bisiaux, M., Brook, E. J., Buizert, C., Caffee, M. W., Dunbar, N. W., Edwards, R.,
594 Geng, L., Iverson, N., Koffman, B., Layman, L., Maselli, O. J., McGwire, K., Muscheler, R., Nishiizumi, K.,
595 Pasteris, D. R., Rhodes, R. H., and Sowers, T. A.: The WAIS Divide deep ice core WD2014 chronology – Part 2:
596 Annual-layer counting (0–31 ka BP), *Climate of the Past*, 12, 769–786, <https://doi.org/10.5194/cp-12-769-2016>,
597 2016.

598 Simon, Q., Thouveny, N., Bourlès, D. L., Nuttin, L., Hillaire-Marcel, C., and St-Onge, G.: Authigenic $^{10}\text{Be}/^{9}\text{Be}$
599 ratios and ^{10}Be -fluxes (^{230}Th s-normalized) in central Baffin Bay sediments during the last glacial cycle:
600 Paleoenvironmental implications, *Quat Sci Rev*, 140, 142–162, <https://doi.org/10.1016/j.quascirev.2016.03.027>,
601 2016.

602 Sinnl, G., Adolphi, F., Christl, M., Welten, K. C., Woodruff, T., Caffee, M., Svensson, A., Muscheler, R., and
603 Rasmussen, S. O.: Synchronizing ice-core and U/Th timescales in the Last Glacial Maximum using Hulu Cave
604 ^{14}C and new ^{10}Be measurements from Greenland and Antarctica, *Climate of the Past*, 19,
605 <https://doi.org/10.5194/cp-19-1153-2023>, 2023.

606 Southon, J.: A first step to reconciling the GRIP and GISP2 Ice-core chronologies, 0-14, 500 yr B.P., *Quat Res*, 57,
607 <https://doi.org/10.1006/qres.2001.2295>, 2002.

608 Spielhagen, R. F., Erlenkeuser, H., and Siebert, C.: History of freshwater runoff across the Laptev Sea (Arctic)
609 during the last deglaciation, *Glob Planet Change*, 48, 187–207, <https://doi.org/10.1016/j.gloplacha.2004.12.013>,
610 2005.

611 Stuiver, M., Pearson, G. W., and Braziunas, T.: Radiocarbon Age Calibration of Marine Samples Back to 9000 Cal
612 Yr BP, *Radiocarbon*, 28, <https://doi.org/10.1017/s0033822200060264>, 1986.

613 Svensson, A., Dahl-Jensen, D., Steffensen, J. P., Blunier, T., Rasmussen, S. O., Vinther, B. M., Vallelonga, P.,
614 Capron, E., Gkinis, V., Cook, E., Astrid Kjær, H., Muscheler, R., Kipfstuhl, S., Wilhelms, F., Stocker, T. F.,
615 Fischer, H., Adolphi, F., Erhardt, T., Sigl, M., Landais, A., Parrenin, F., Buizert, C., McConnell, J. R., Severi,
616 M., Mulvaney, R., and Bigler, M.: Bipolar volcanic synchronization of abrupt climate change in Greenland and
617 Antarctic ice cores during the last glacial period, *Climate of the Past*, 16, [https://doi.org/10.5194/cp-16-1565-](https://doi.org/10.5194/cp-16-1565-2020)
618 2020, 2020.

619 Wittmann, H., von Blanckenburg, F., Mohtadi, M., Christl, M., and Bernhardt, A.: The competition between coastal
620 trace metal fluxes and oceanic mixing from the $^{10}\text{Be}/^{9}\text{Be}$ ratio: Implications for sedimentary records, *Geophys*
621 *Res Lett*, 44, <https://doi.org/10.1002/2017GL074259>, 2017.

622 Wollenburg, J. E. and Kuhnt, W.: The response of benthic foraminifers to carbon flux and primary production in
623 the Arctic Ocean, in: *Marine Micropaleontology*, [https://doi.org/10.1016/S0377-8398\(00\)00039-6](https://doi.org/10.1016/S0377-8398(00)00039-6), 2000.

624 Wollenburg, J. E. and Mackensen, A.: On the vertical distribution of living (Rose Bengal stained) benthic
625 foraminifers in the Arctic Ocean, *J Foraminifer Res*, 28, <https://doi.org/10.2113/gsjfr.28.4.268>, 1998.

626 Wollenburg, J. E., Matthiessen, J., Vogt, C., Nehrke, G., Grotheer, H., Wilhelms-Dick, D., Geibert, W., and
627 Mollenhauer, G.: Omnipresent authigenic calcite distorts Arctic radiocarbon chronology, *Commun Earth*
628 *Environ*, 4, <https://doi.org/10.1038/s43247-023-00802-9>, 2023.

629 Yiou, F., Raisbeck, G. M., Baumgartner, S., Beer, J., Hammer, C., Johnsen, S., Jouzel, J., Kubik, P. W.,
630 Lestringuez, J., Stiévenard, M., Suter, M., and Yiou, P.: Beryllium 10 in the Greenland Ice Core Project ice core
631 at Summit, Greenland, *J Geophys Res Oceans*, 102, <https://doi.org/10.1029/97JC01265>, 1997.

632 Zheng, M., Liu, H., Adolphi, F., Muscheler, R., Lu, Z., Wu, M., and Prisle, N. L.: Simulations of ^7Be and ^{10}Be
633 with the GEOS-Chem global model v14.0.2 using state-of-the-art production rates, *Geoscientific Model*
634 *Development Discussions*, <https://doi.org/10.5194/gmd-2023-111>, 2023.